ISME

Wind Farm Layout Optimization using a Reynolds-averaged Navier–Stokes Model and a Genetic Algorithm

A. Pourrajabian[*]
Assistant Professor

R. Ebrahimi[†]
Professor

M. Rahmanpour[‡]
Assistant Professor

S. Rahgozar[§]
Assistant Professor

M. Dehghan[**]
Assistant Professor

The placement of wind turbines in a wind farm can considerably affect the total output power. Using computational fluid dynamics and genetic algorithm, the optimal arrangement of turbines in a given wind farm was determined. A three-dimensional Reynolds-averaged Navier-Stokes simulation was conducted on a 660 kW three-bladed horizontal axis turbine. The airflow was assumed to be steady state and a pressure-based approach was adopted to solve the governing equations. By employing the characteristics of the wake propagation, the appropriate distances between the adjacent turbines were calculated. To find the optimal placement of the turbines, a purpose-built genetic algorithm was employed. The results show that the final configuration is in line with the outcomes of the previous study. The sensitivity analysis of the genetic algorithm with respect to its parameters was also performed to guarantee that the final layout is an optimal one.

DOI: 10.30506/jmee.2020.112337.1194

Keywords: Wind farm layout, Optimization, RANS, Genetic algorithms

1 Introduction

The determination of the wind turbines arrangement is one of the most important steps in the implementation of a wind farm project; since it significantly affects both the cost and the output power of the farm. The latter is strongly influenced by wind turbines configuration while the former mainly depends on the number of turbines [1-3]. A dense arrangement may lead to the reduction of the output power as the kinetic energy of the wind falls noticeably behind upstream turbines, which can diminish the energy production of downstream.

A sparse arrangement, on the other hand, may not be of interest as it significantly increases the infrastructure cost. Hence, there appears to be a trade-off between the total cost and the total output power. More importantly, the output power not only is affected by the farm arrangement, it is also affected by the topography of the terrain, the wind farm area, turbines size, wind speed/direction, to name but a few [1-4]. To address the aforementioned wind farm layout problem, a number of optimization techniques have been widely developed and employed by several researchers [5-18]. Mosetti et al. [5] employed the genetic algorithm (GA) to find the optimal placement of the wind turbines in a wind farm with an area of 4 km^2.

[*] Corresponding Author, Assistant Professor, Department of Energy, Materials and Energy Research Center (MERC) a.pourrajabian@merc.ac.ir

[†] Professor, Faculty of Aerospace Engineering, KNToosi University of Technology rebrahimi@kntu.ac.ir

[‡] Assistant Professor, Department of Mechanical Engineering, Azarbaijan Shahid Madani University

[§] Assistant Professor, Department of Energy, Materials and Energy Research Center (MERC)

[**] Assistant Professor, Department of Energy, Materials and Energy Research Center (MERC)

Receive : 2019/08/01 Accepted : 2020/03/08

Depending on the wind characteristics, they considered three cases, namely single wind direction, constant intensity with variable wind direction, and variable intensity with variable wind direction. The same problem was further investigated by Grady et al. [6] and different optimal arrangement was reported. The discrepancy was found to be attributed to the values of GA parameters and also the algorithm convergence [6]. Paying more attention to details of the wind farm cost, Elkinton et al. [7] used a greedy heuristic and GA to design the layout of an offshore wind farm. The cost was divided into several sub-components including major costs, e.g. turbines, electrical interconnection, maintenance and cost of energy production and energy losses [7]. An evolutionary algorithm (EA) was employed by Gonzalez et al. [8] to optimize the layout of wind farms. Compared to other studies, their proposed cost model was comprehensively described in more detail, considering the wind speed/direction distributions and the technical parameters of the wind turbines such as the rated power and the tower height. Moreover, the loss production of the wind farm due to the wake effects, the auxiliary costs including foundations, road infrastructure and buildings, substation and wind farm electrical network were also taken into account. Of particular interest is that the convergence rate of the proposed algorithm was faster than the similar studies [8]. Emami and Noghreh [9] introduced a novel approach to address the wind farm layout problem. A new objective function consists in weighting coefficients was defined, and the three conventional cases, introduced by Mosetti et al. [5], were addressed. In a completely different scheme, Marmidis et al. [10] employed the Monte Carlo simulation to find the optimal arrangement of turbines. Having simulated the problem for the uniform velocity with constant direction, they found a completely different layout with respect to Mosetti et al. [5] and Grady et al. [6]. More importantly, their results show that more output power is achievable not necessarily by using more turbines in wind farms [10]. Gonzalez et al. [11] introduced a new tool, which integrates the performance of two nested evolutionary algorithms. The first and main EA calculates the turbines layout, wind turbine type, tower height and the inner auxiliary road of the wind farm. It also controls the performance of the second EA that optimizes the design of the electrical infrastructure. The cost model consisted of production, losses, operation and maintenance, and the final removing cost.

Also included in this optimization scheme were some constraints, including the forbidden zones, transmission line capacity and initial investment [11]. In addition to the technical parameters of the turbine, the land restrictions such as prohibited zones and the capacity of soil could also affect the placement of wind turbines in a wind farm [12]. Those factors were addressed in a study carried out by Rahbari et al. [12] who applied a novel placement selector approach for the realistic design of wind farm layouts, which resulted in an efficiency improvement of 3%. A new metric based on the power surface of wind farms was introduced by Feng and Shen [13] for the wind farm layout optimization. Considering both short-term and long-term wind condition variations, the trade-offs between high mean value and low variability of output power were addressed in the study [13]. Using particle swarm optimization, Wan et al. [14] introduced a new approach for the placement of wind turbines in a continuous space of a wind farm. The optimization procedure aimed at maximizing the output power of a farm with a fixed number of turbines and with the minimal distance between them [14]. Chen et al. [15] optimized the placement of wind turbines with different hub height in a two-dimensional area. Compared to the single hub height wind turbines, results indicated that output power of the wind farm using different hub height wind turbines would be increased with the same number of wind turbines [15]. Layout optimization of wind farms with regular and irregular shapes was done by Chen et al. [16]. The study revealed that by appropriate choosing of different type and hub height of wind turbines, better results are achievable [16]. In Kusiak et al. [17], the constraints were transformed into a second objective function since the layout design of wind turbines is a constrained optimization problem. A multi-objective evolutionary algorithm was then developed to solve the transformed optimization problem, which simultaneously

maximized the output power and also minimized the constraint violations [17]. In a different study, the role of landowners in a system-level wind farm layout optimization was investigated by Chen and MacDonald [18]. In this study, a cost-of-energy model with realistic landowner remittances was developed, which could help site developers for optimal placement of wind turbines [18]. Micro-siting of large-scale wind farms was carried out by Song et al. [19] who employed a two-level optimization approach for the layout problem. It consists of a hierarchical structure where the wind farm was considered as a compound that consists of several blocks. Thereafter, a multi-objective algorithm was employed to optimize the wind farm which resulted in more power and less cost [19]. For large-scale wind farms, the economic aspects are of utmost importance. Wu et al. [20] applied the cable routing for power transmission and also the economic benefit during the optimization which was done by GA. The levelized cost of energy (LCOE) was considered as the primary objective function for the grid-based wind farm layout optimization [21]. For that purpose, the effect of turbine type, the number of turbines and the rotor diameter were fully studied. Results indicated that improving the capacity factor does not result in decreasing LCOE. In an attempt to reduce the computational time of layout optimization, the simulated annealing (SA) technique was adopted for the placement of the turbines in a wind farm [22]. Based on the different scenarios, results showed that the SA could be considered as a suitable option for the wind farm layout optimization problem [22]. The aim of the present study is to provide an engineering tool for the wind farm layout optimization. The simple wake model based on the momentum balance and Betz theory has been widely used in the previous studies [5, 6, 10]. Solutions based on the computational fluid dynamics (CFD) have an advantage and potential to predict more accurate results. In other words, it is expected that solving all governing equations without any simplicity would lead to more accurate outcomes. In this regard, the Reynolds-averaged Navier-Stokes (RANS) simulation is conducted on a 660 kW three-bladed horizontal axis wind turbine. Afterwards, the suitable distances between turbines are determined and an engineering expression is proposed for the wake propagation. Those results will be used in the optimization part of the study, where the GA is employed to find the optimal arrangement of wind turbines in a wind farm.

2 Computational methodology

ANSYS Fluent [23] was used for the simulation of wind turbine. Although direct numerical simulations (DNS) and large-eddy simulations (LES) could provide very accurate results at considerable expense of the computational time and cost, the Reynolds-averaged Navier-Stokes (RANS) models are acceptable alternatives for wind turbines simulation [24-26]. The RANS form of the conservation equations including the mass and momentum can be written as follows:

$$\frac{\partial(\rho\bar{u}_i)}{\partial x_i} = 0 \tag{1}$$

$$\frac{\partial}{\partial x_j}\left(\rho\bar{u}_i\bar{u}_j + \rho\overline{u_i'u_j'}\right) = -\frac{\partial\bar{p}}{\partial x_i} + \frac{\partial\bar{\tau}_{ij}}{\partial x_j} \tag{2}$$

Where ρ is the air density and $\bar{p}$ is the mean pressure. Note that the Einstein summation convention applies. Also, $\bar{u}_i$ is the mean velocity tensor of the fluid flow, u_i' is the fluctuating component of velocity and $\bar{\tau}_{ij}$ represents the mean viscous stress tensor components:

$$\bar{\tau}_{ij} = \mu\left(\frac{\partial\bar{u}_i}{\partial\bar{x}_j} + \frac{\partial\bar{u}_j}{\partial x_i}\right) \tag{3}$$

here, μ is the dynamic viscosity. By employing the "moving reference frame" feature of ANSYS Fluent, the problem can be converted from an unsteady state to a steady one. The first order upwind scheme was employed for discretization of momentum equations and the pressure-velocity coupling was performed by means of SIMPLE technique [23].

Because of the rotation and also the sharp curvature of the surfaces, the separation is inevitable in turbo-machinery problems. To appropriately capture the flow field, the Shear Stress Transport (SST) k-ω model was selected for the turbulence modeling. It is a two-equation model for the turbulence kinetic energy (k) and the specific dissipation rate (ω). It is argued that the capability of SST k-ω for the prediction of separation at adverse pressure gradients is more accurate than the standard k-ε and k-ω models [27]. In fact, the k-ε model performs poorly in adverse pressure gradients while the k-ω model overpredicts the level of shear stress. The SST k-ω model, however, is a combination of those models and switches between them based on the distance from walls. While the k-ω model predicts well the near-wall region, the k-ε model is more suited away from the wall [27]. The mathematical description of SST k-ω can be found in [23, 27]. It should be noted that the default values of the SST k-ω model constants in ANSYS Fluent [23] remained unchanged.

2.1 Grid generation

Figure (1) shows the wind turbine blade studied in the present study. The blade radius is 23 m and it consists of a variety of airfoils as summarized in Table (1). Also provided are the chord values and twist angle; the angle between the plane of rotation and the chord line, Table (1).
It is worth noting that the blade cross-section is converted into the elliptical and circular sections in order to connect the blade to the turbine hub, Figure (1). Due to the periodic rotation of the blade, one blade was simulated, and the nacelle and tower were excluded from the simulation. A truncated cone with 120^{o} sector was considered as the computational domain. The length of computational domain is 12D, with D equals the rotor diameter of the turbine, Figure (2). The location of the wind turbine in the central plane of the computational domain is shown in Figure (2). As shown, the domain is three-fold larger in the upstream and nine-fold larger in the downstream. A combination of the hexahedral and tetrahedral elements was generated in the computational domain. The blade was surrounded by a thin volume in which the high-resolution hexahedral elements were generated, Figure (3) and Figure (4). Figure (5) shows the two sides of the computational domain where the generated triangle elements in those planes is identical. This is due to the assigning the periodic boundary condition to those planes which will be discussed later.

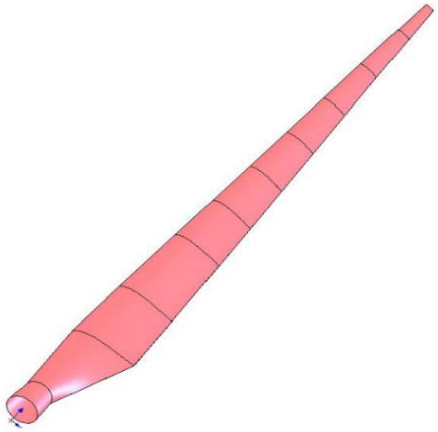

Figure 1 The schematic of the wind turbine blade.

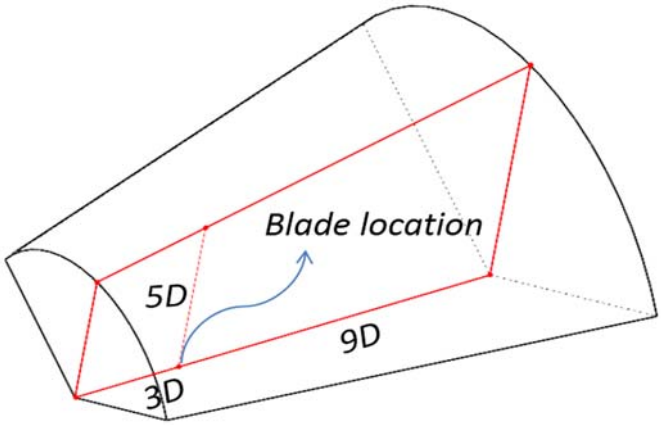

Figure 2 The location of the wind turbine blade in the central plane of the computational domain (D is the rotor diameter).

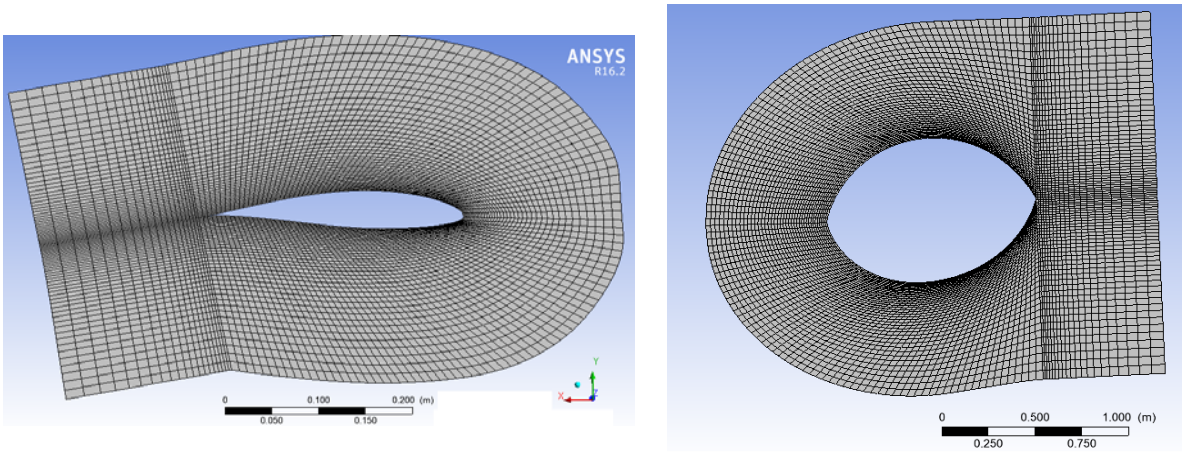

Figure 3 The generated grid around the blade tip (left) and near the root (right).

Table 1 Geometrical parameters of the blade [28].

Blade radius (m)	5-11	12-15	16-20	21	22	23
Airfoil type	FFA-W3	mix	NACA-63-600	NACA-63-450	NACA-63-330	NACA-63-150
Chord (mm)	2040-1470	1375-1090	995-615	520.5	425	330
Twist angle (deg.)	13.5-5.1	4.5-2.8	2.3-0.6	0.3	0.07	0

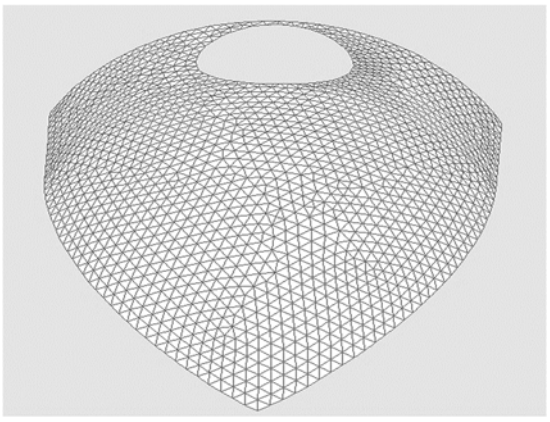

Figure 4 The generated grid over the wind turbine nose.

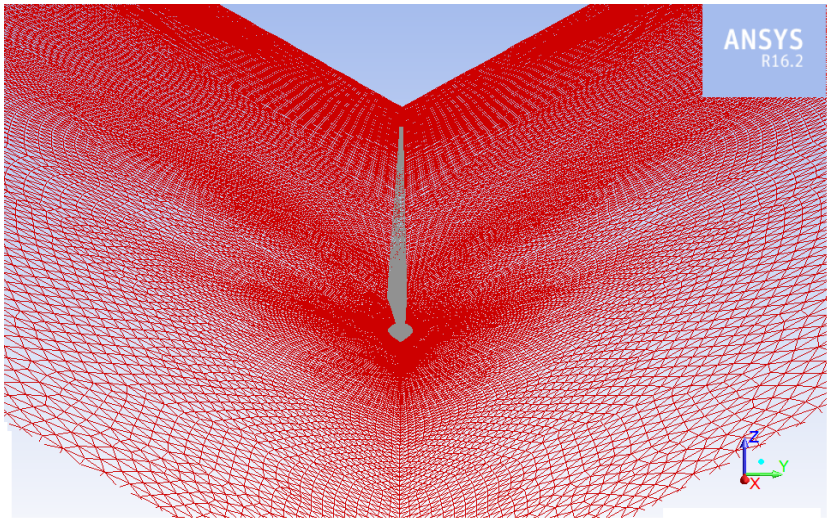

Figure 5 The computational grids in the lateral planes of the domain.

To appropriately using the SST *k-ω* model, the closest mesh node to the wall should be located below $y^+ = 5$ [23, 27], where y^+ is the distance from the wall normalized by inner scales as follows:

$$y^+ = u^* y/v \tag{4}$$

Where u^* is the friction velocity, v is the kinematic viscosity, and y is the wall distance in physical unit. In this regard, the assessment of mesh resolution was performed by computing the y^+ values along the blade. In addition to y^+ values, the turbine output power and the velocity profile downstream the turbine were monitored for the grid convergence study. For this purpose, the grid density was increased entire the computational domain and particularly near the blade surfaces. The results will show that with 14.7×10^6 computational cells, the velocity profile downstream the turbine remains virtually unchanged.

2.2 Operating and boundary conditions

The technical parameters of the 660 kW wind turbine which is widely used in the wind farms of Iran are listed in Table (2). The rated wind speed of 15 m/s was assigned to the front of the computational domain and also above of it, Figure (2). The free stream pressure was considered at the outlet of the computational domain and the periodic boundary condition was applied in the lateral planes, Figure (5).

2.3 Wake model

Accurate modeling of the wake propagation downstream of a wind turbine is a formidable task. Downstream the wind turbine can be divided into two main regions, namely the near and the far wake. The length of former is approximately 1D where the effects of tip vortices are important but for the latter, the wake effects could propagate up to 20D [29]. Modeling the wake area has been carried out both numerically and experimentally [30-34]. Numerical techniques such as large eddy simulation have been widely employed [32-34]. Experimental investigations, on the other hand, have been also conducted to capture the far wake region in more detail [31-32]. However, a time-consuming process must be done for the implementation of both approaches.

To address that issue, engineering expressions have been proposed for the early stages of the wind farm design of which, the following equation describes the velocity deficit in the far wake region [29]:

$$\Delta V = V_{hub} A(R/x)^n \tag{5}$$

where V_{hub} is the wind speed at the hub height and ΔV is the difference between V_{hub} and the wind speed at x position in the downstream. Also, R is the blade radius, A and n are unknown constants, which are very sensitive to the type of the turbine [29].

In a wind farm, the velocity in the wake of upstream turbine can be found by Eq. (5), provided that A and n are known. However, when a turbine encountering multiple wakes, the kinetic energy of the mixed wake can be assumed to be equal to the sum of kinetic energy deficits, which led to the velocity, $\bar{U}$, for the downstream turbines [5-6]:

$$(\text{Deficit}_{\text{Total}})^2 = \sum_{\text{Turbines}} (\text{Deficit}_i)^2 \rightarrow \left(1 - \frac{\bar{U}}{U_\infty}\right)^2 = \sum_{\text{Turbines}} \left(1 - \frac{U_i}{U_\infty}\right)^2 \tag{6}$$

or

$$\bar{U} = U_\infty \left[1 - \sqrt{\sum \left(1 - \frac{U_i}{U_\infty}\right)}\right] \tag{7}$$

Having $\bar{U}$, the output power is then calculated from [2-3]:

$$P = 0.5 C_p \rho S \bar{U}^3 \tag{8}$$

where C_p is the power coefficient and S the swept area of the blades. Figure (6) shows C_p over the range of wind speed for the considered turbine.

Table 2 Main parameters of the considered wind turbine [28].

Parameter	Value
Rated power	660 kW
Rotor speed	28.5 RPM
Blade radius	23 m
Tower height	40 m
Cut-in speed	4 m/s
Rated speed	15 m/s
Cut-out speed	25 m/s

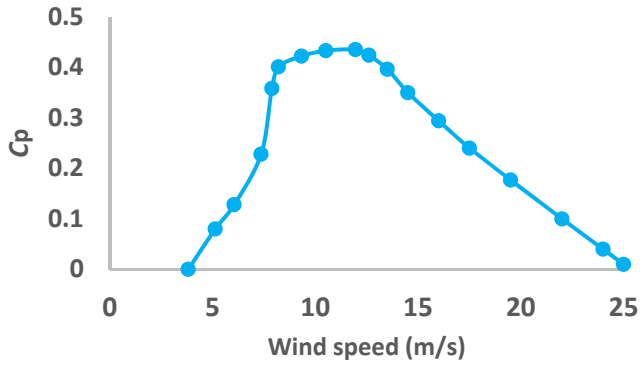

Figure 6 Power coefficient (C_p) variation with wind speed for the considered turbine.

3 Genetic algorithms (GA) for optimization

Developing on the basis of the natural evolution, GA is one of the most famous evolutionary algorithms, which has been employed in science and engineering problems [35]. In order to implement GA, the problem variables, known also as "chromosomes", is first encoded into the genetic space either in binary or continuous form, and the population matrix is randomly generated. Then, the three standard operators, namely selection, crossover and mutation are employed to determine the optimal solution of an optimization problem. To that end, the objective function is calculated for all chromosomes. Thereafter, the best of them, determined by the selection rate, are kept as parents to produce new offspring (here new layouts), determined by the crossover operator, and the others are discarded. Finally, with the help of mutation operator, the algorithm effectively explores the solution space [35]. In order to find the optimal solution, the GA cycle is repeated through the large number of generations until a convergence criterion is met [35]. The binary GA is a pertinent choice for the optimization of the wind farm layout problem. Figure (7) shows how the wind farm layout is encoded into the binary space. The values of the GA parameters used here are listed in Table (3).

The following objective function was considered for the optimization:

$$\text{Objective function} : \text{Min}\left(\frac{\text{Cost}_{\text{total}}}{P_{\text{total}}}\right) \tag{9}$$

where P_{total} is the total output power of the wind farm and $\text{Cost}_{\text{total}}$ is the wind farm cost. Indeed, minimization of that function leads to a maximum energy for a minimum cost. Note that the total power of a wind farm is equal to the summation of power harnessed by each turbine:

$$P_{\text{total}} = \sum_{i=1}^{N_t} P_i \tag{10}$$

where P_i is calculated for each turbine from Eq. (8).
Assuming that a large number of turbines are installed in the wind farm, the following model was applied for the cost function, which considers the non-dimensional cost of one for a single turbine with the maximum reduction of 1/3 for extra turbines [5-6]:

$$\text{Cost}_{\text{total}} = N_t\left(\frac{2}{3}+\frac{1}{3}e^{-0.00174\,N_t^2}\right) \tag{11}$$

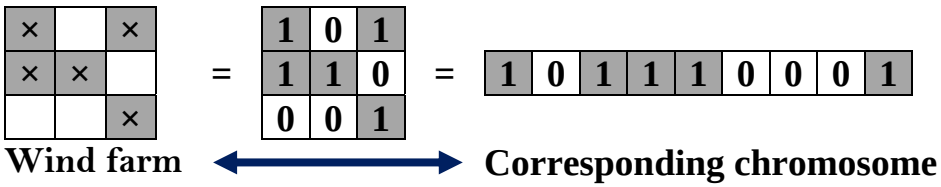

Figure 7 Encoding the wind farm layout into a chromosome.

Table 3 Values of the GA parameters.

Parameter	Population Size	Crossover rate	Mutation rate
Value	100	0.5	0.1

Where N_t is the number of turbines, which is an unknown parameter that should be determined through the optimization procedure. Although the total power is affected by N_t, the results will show that the wind farm arrangement is the decisive factor.

4 Results and discussion

The first parts of this section deal with the numerical results of the CFD investigation including the velocity distribution, the grid study and also the applied wake model results. Thereafter, these outcomes will be used in the optimization part of the study, where the optimal layout of the wind farm will be determined.

Figure (8) shows the velocity distribution downstream of the wind turbine. While the velocity values drop noticeably in the near wake region and just behind the blade, it gradually begins to increase towards the end of computation domain. In fact, moving from the wind turbine and in the far wake region; the velocity approaches to the free stream velocity because of the penetration of the fluid momentum. In order to assess the grid independency of the results, velocity profile downstream of the turbine was evaluated for two grids namely Grid1 and Grid2; Figure (9). Note that the Z is an axis along the wind turbine blade, Figure (5) and Figure (8). As shown, the profiles are almost identical and, as expected and highlighted in Figure (9), the reduction in velocity reduces far from the turbine which was already shown in Figure (8). It should be noted the trend of velocity profiles shown in Figure (9) is consistent with the measured values of other studies. For example, see Figure (36) of [29].

4.1 Wake model results

Velocity profiles behind the wind turbine for four locations are shown in Figure (10). Far from the turbine and in the far wake region, the velocity profile is approximately uniform while this in not the case in the near wake area. That is due to the tip vortices and their interactions together with the three-dimensional effects right after the turbine. On the other hand, in the far wake region, those effects no longer play a major role and, as a result, the wind velocity becomes uniform, Figure (10). The unknown parameters of the applied wake model, Eq. (5), were calculated by employing the method of least squares. Figure (11) depicts the variations in velocity magnitude downstream of the turbine, and Figure (12) shows how the wake propagates downstream of the wind turbine. The slope of wake region (α) downstream of the turbine can be assessed by the following empirical relation [5-6]

$$\alpha = 0.5 / \ln\left(z / z_0\right) \tag{12}$$

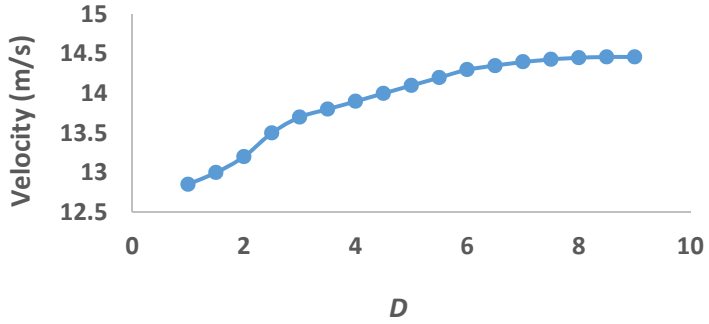

Figure 8 Average velocity downstream of the blade (D is the rotor diameter).

Where z_0 is the surface roughness and z is the height of turbine tower. The calculated slope (0.12) shown in Figure (12) is very close to α= 0.102 by applying 0.3 for z_0 [2-3], and 40 m for z, Table (2). Based on the results shown in Figure (11), the variations in wind velocity are not pronounced between 7D and 9D. More specifically, the deficit rate remained almost unchanged from 8D to 9D. Taking into account the trend of velocity profile shown in Figure (10), 8D was selected as the distance between the turbines which is in the range of 8D to 10D, recommended by the researchers for the windward direction in wind farms [3].

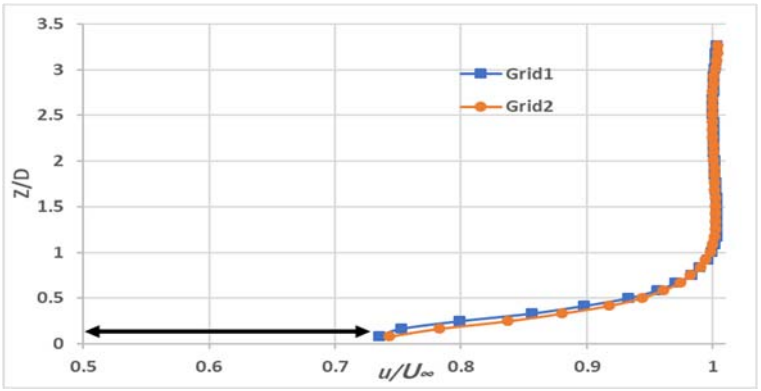

i) D

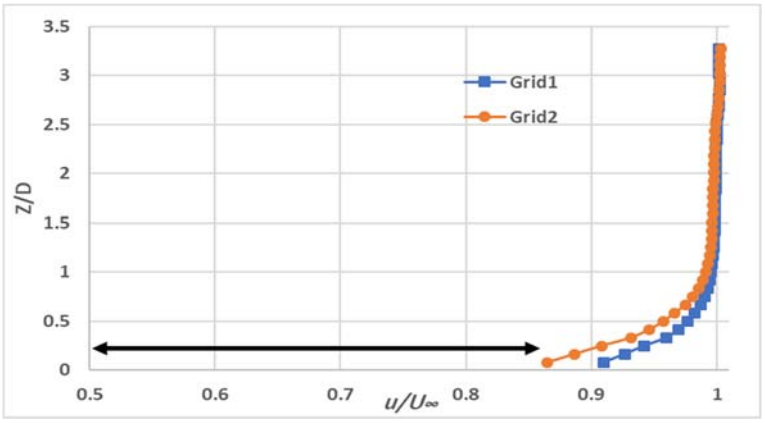

ii) 3D

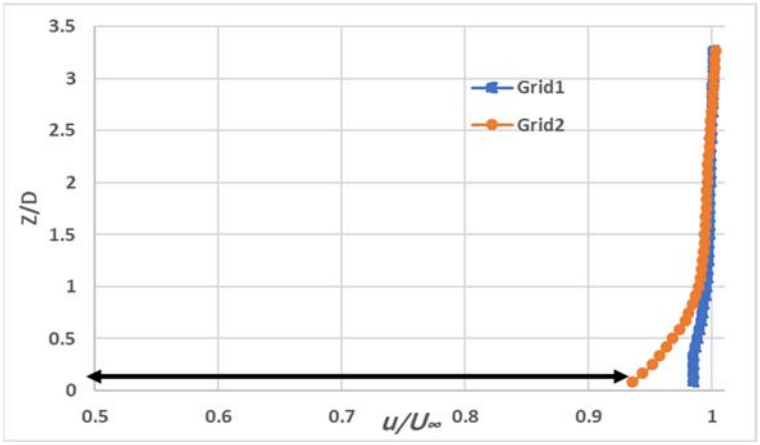

iii) 6D

Figure 9 Velocity profiles downstream of the turbine (Grid1=7.1×10^6 cells, Grid2=14.7×10^6 cells).

4.2 Optimal placement of the wind turbines

Similar to that reported in [5, 6, 10, 22], a wind farm with 100 square cells was selected for the optimization procedure. Figure (13) shows the optimal placement of the wind farm in which each column consists of 5 turbines. The best and also the mean fitness (objective) function values during the GA cycle are shown in Figure (14). The oscillating trend of the mean fitness values is due to the different combination of the possible solutions in the population matrix in each generation.

The sensitivity analysis of the GA with respect to its parameters was done extensively. To that end, the optimization procedure was repeated with the different population size of 50, 75 and 100 and also the mutation rate of 0.1, 0.15 and 0.2. These two parameters were selected on the basis that they are the decisive parameters in the sensitivity analysis of the GA [35]. It should be noted that in all the cases, the similar arrangement shown in Figure (13) was reached.

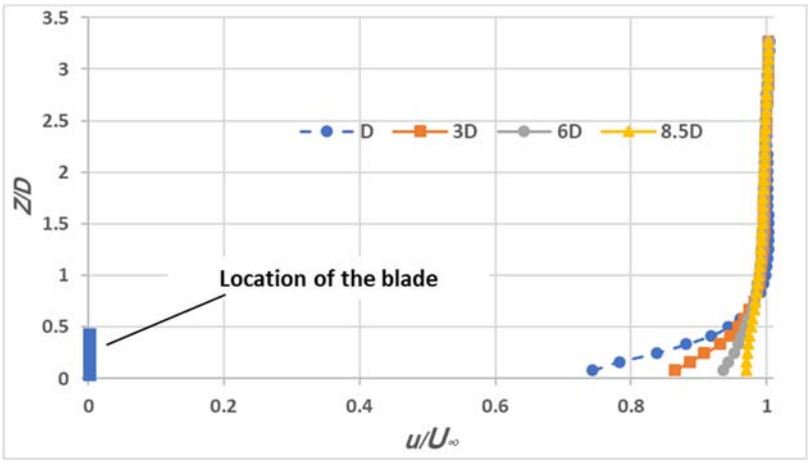

Figure 10 Velocity profile downstream of the turbine.

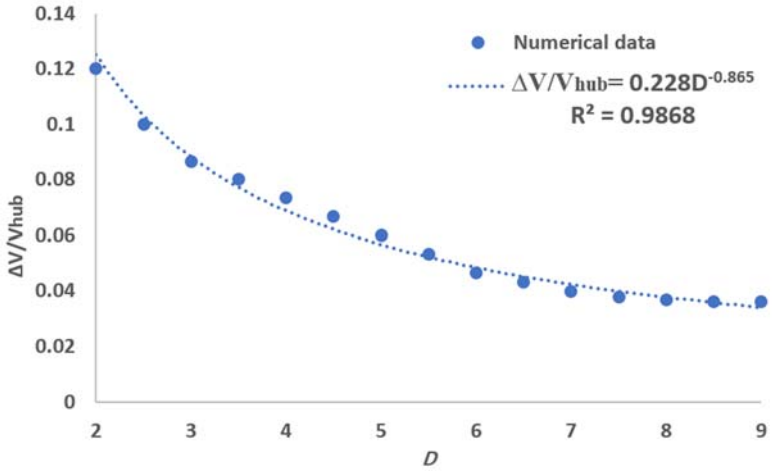

Figure 11 Variations in wind velocity downstream of the turbine using the applied wake model; Eq. (5).

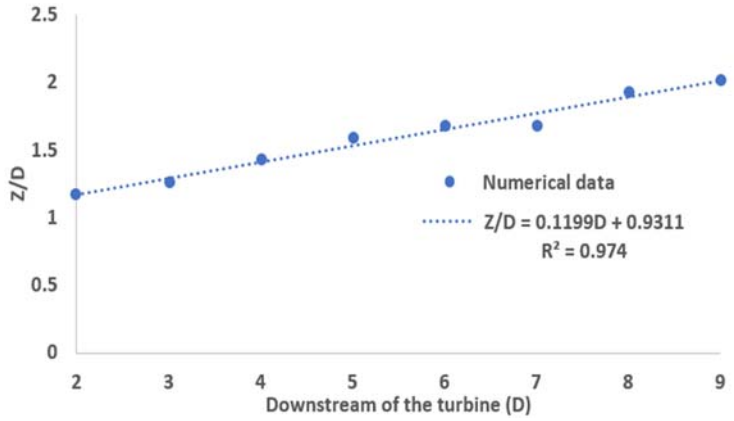

Figure 12 The propagation of the wake downstream of the turbine.

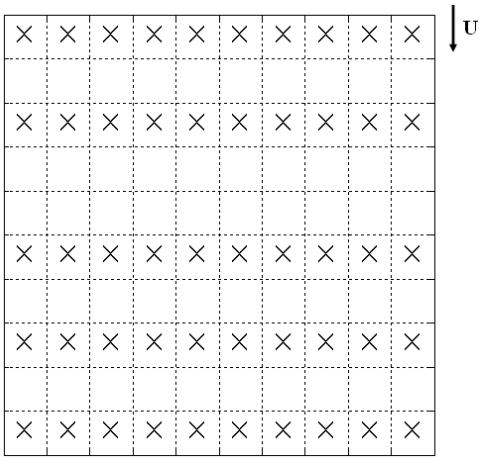

Figure 13 The optimal placement of the wind farm.

In order to assess the optimal arrangement, a random placement for turbines was considered, Figure (15). Table (4) compares the characteristics of the random and optimal arrangements. Because of a larger number of turbines in the random layout (i.e. 64), the corresponding output power is higher than the optimal one. However, the objective function value for the latter is smaller. This highlights that the arrangement of wind turbines is more important than the number of turbines in a wind farm. Also provided in Table (4) is the wind farm efficiency, which is the ratio of the total power of a wind farm to the summation of the rated power of each turbine without considering the wake interactions. This table shows that the efficiency of the optimal arrangement is only slightly greater than that of the random one.

The fact that the efficiency of the random layout is as high as that of the optimal one deserves an explanation here. The distance between the cells found in this study was sufficiently large, leading to the recovery of the wind speed right after each turbine. Since the output power is proportional to the cubic of velocity, the recovery of the wind speed results in higher power, and consequently high efficiency of the random arranged wind farm.

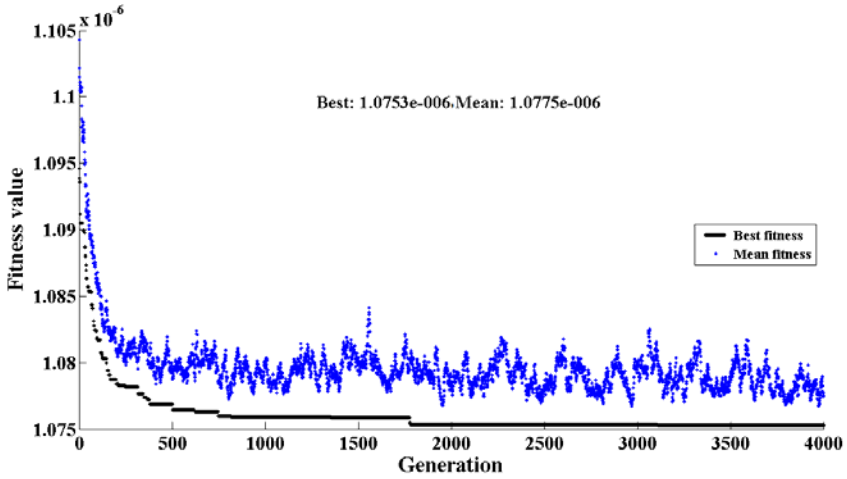

Figure 14 The best/mean fitness value during the GA cycle.

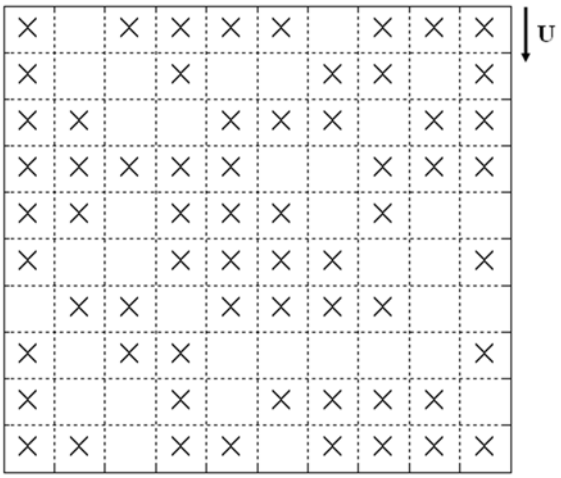

Figure 15 The layout of random placement.

Table 4 The comparison between the optimal layout and the random one.

	P_{total} (MW)	fitness value	(N_t)	Efficiency (%)
Random layout, Figure (15)	38.58	1.10630e-6	64	91
Optimal layout, Figure (13)	31.2	1.07528e-6	50	94.5

In order to further discuss the results, the optimal layouts reported in Mosetti et al. [5] and Grady et al [6] are shown in Figure (16) for the constant variable and direction of the wind. Table (5) compares the results of these studies with those of the present study. The rotor diameter of the turbines is approximately the same but the cell distance is different, Table (5). The fitness improvement of Grady et al. [6] over the Mosetti et al. [5] was attributed to the values of GA parameters. More specifically, the population size and number of generations applied in [6] were respectively 600 and 3000, which are noticeably larger than 200 and 400 used in [5]. Compared to Grady et al. [6], the optimal layout of this study is slightly different, Figure (13) and Figure (16). That is mainly due to the distance between the cells in the wind farm. By considering the larger distance (8D), the algorithm found more turbines in each column due to the recovery of the wind speed, which led to a higher output power. Although the large number of turbines would increase the wind farm cost, the corresponding power would increase as well. Since the increase in the output power exceeds the incremental cost, the fitness value in this study is smaller than that in [5, 6], Table (5).

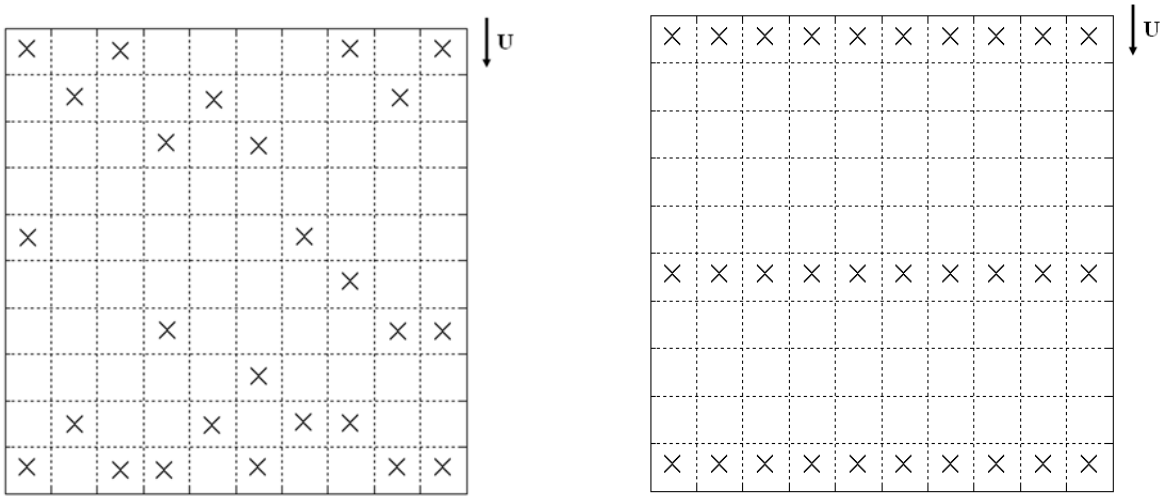

Figure 16 The optimal placement of the wind farm: Mosetti et al. [5] (left) and Grady et al. [6] (right).

Table 5 The comparison between the present study, Mosetti et al. [5] and Grady et al. [6].

	Turbine Diameter (m)	Cell distance	Wind velocity (m/s)	Number of turbines	Efficiency (%)	Fitness value
Mosetti et al. [5]	40	5D	12	26	91.645	1.6197e-3
Grady et al. [6]	40	5D	12	30	92.015	1.5436e-3
Present Study	46	8D	15	50	94.5	1.0753e-6

4.3 Effect of intensity and direction of the wind

In a real wind farm, the wind velocity and its direction vary hourly. In fact, in realistic situations, there are more than one wind direction with the different probability that should be considered in the wind farm design. To assess the effect of these parameters on the wind farm layout, the optimization procedure was repeated based on the occurrence of the velocity values and the wind direction. Figure (17) shows the variation in the wind velocity and also the wind direction. This distribution was used by majority of the researchers [5-6, 22]. For this case, the output power is calculated by considering the fraction of occurrence, f, as:

$$P=0.5fC_p\rho S\,\bar{U}^3 \tag{13}$$

Figure (18) shows the optimal placement with 46 turbines for this case. In the north-south direction, there is a small similarity between this placement and that of Figure (13). However, the different placement is pronounced especially at the center of the wind farm, Figure (13) and Figure (18). As can be seen, the arrangement of the turbines in this case is focused on the northwest direction where the occurrence of the wind is much larger than the other directions, Figure (17) and Figure (18). This led to the dense placement far from the wind farm center and in the top corners. On the other hand, the sparse placement was found by the GA in the center of the wind farm.

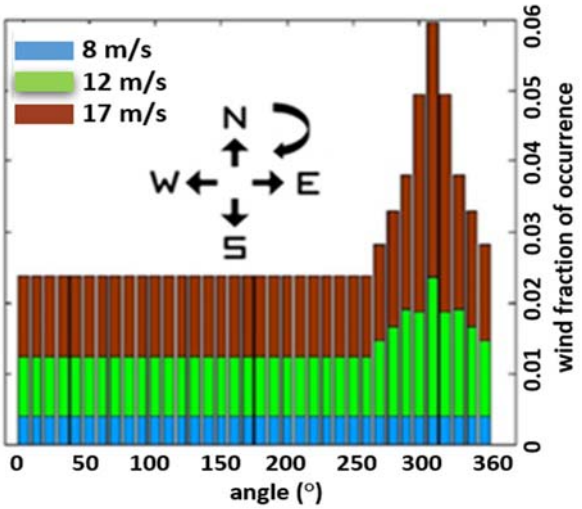

Figure 17 The wind fraction of occurrence with respect to the velocity and direction [5-6, 22].

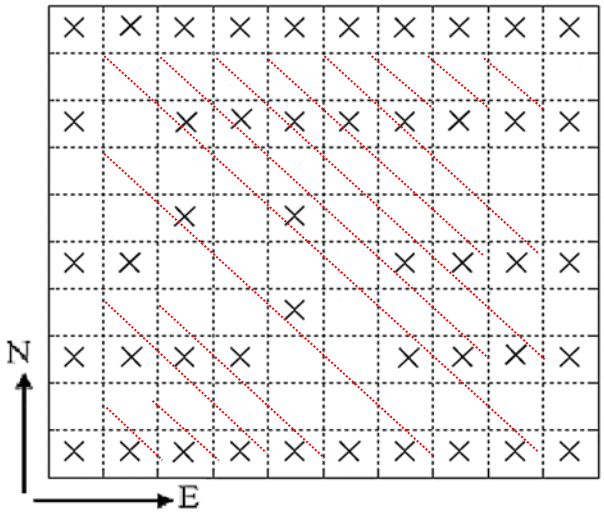

Figure 18 The optimal placement of the wind farm based on the conditions of Figure (17).

5 Conclusions

The arrangement of wind turbines in wind farms has a considerable effect on the energy yield harnessed by turbines. The computational fluid dynamics in conjunction with the genetic algorithm was employed to find the optimal layout of a wind farm. The first part of the study dealt with the investigation of flow field around the 660 kW horizontal axis wind turbine which was done using ANSYS Fluent. Applying the Reynolds-averaged Navier-Stokes form of the governing equations, the wind velocity downstream of the turbine was calculated and a handy expression was proposed and validated which describes the wake propagation and also the wind velocity from the near wake area to the far wake region. In the second part of the study, the genetic algorithm was used to find the optimal placement of turbines. To that end, the optimization algorithm simultaneously maximized the output power and minimized the wind farm cost. The sensitivity analysis of the genetic algorithm with respect to its main parameters including the population size and the mutation rate was carried out. With respect to the outcomes of the previous studies, the optimal arrangement shows the reasonable agreement. While the proposed scheme can be used in the preliminary design of a wind farm, a more realistic cost model is also required to predict the exact cost of the wind farm over its lifetime of typically 20 years.

References

[1] Crespo, A., Hernandez, J., and Frandsen, S., "Survey of Modelling Methods for Wind Turbine Wakes and Wind Farms", Wind Energy, Vol. 2, No. 1, pp. 1-24, (1999).

[2] Manwell, J.F., McGowan, J.G., Rogers, A.L., "*Wind Energy Explained: Theory, Design and Application*", John Wiley and Sons, New York, (2010).

[3] Erich, H., "*Wind Turbines*", 2nd Edition, Springer, Berlin, Germany, (2005)

[4] Milborrow, D.J., "The Performance of Arrays of Wind Turbines", Wind Engineering and Industrial Aerodynamics, Vol. 5, No. 3-4, pp. 403-430, (1980).

[5] Mosetti, G., Poloni, C., and Diviacco, B., "Optimization of Wind Turbine Positioning in Large Wind Farms by Means of a Genetic Algorithm", Wind Engineering and Industrial Aerodynamics, Vol. 51, No. 1, pp. 105-116, (1994).

[6] Grady, S.A., Hussaini, M.Y., and Abdullah, M.M., "Placement of Wind Turbines using Genetic Algorithms", Renewable Energy, Vol. 30, No. 2, pp. 259-270, (2005).

[7] Elkinton, C.N., Manwell, J.F., and McGowan, J.G., "Optimization Algorithms for Offshore Wind Farm Micrositing ", In Proceedings of the WINDPOWER 2007 Conference and Exhibition, Los Angeles, CA, USA, pp. 3-6, (2007).

[8] González, J.S., Rodriguez, A.G.G., Mora, J.C., Santos, J.R., and Payan, M.B., "Optimization of Wind Farm Turbines Layout using an Evolutive Algorithm", Renewable Energy, Vol. 35, No. 8, pp. 1671-1681, (2010).

[9] Emami, A., and Noghreh, P., "New Approach on Optimization in Placement of Wind Turbines within Wind Farm by Genetic Algorithms", Renewable Energy, Vol. 35, No. 7, pp. 1559-1564, (2010).

[10] Marmidis, G., Lazarou, S., and Pyrgioti, E., "Optimal Placement of Wind Turbines in a Wind Park using Monte Carlo Simulation", Renewable Energy, Vol. 33, No. 7, pp. 1455-1460, (2008).

[11] González, J.S., Rodríguez, A.G., Mora, J.C., Payán, M.B., and Santos, J.R., "Overall Design Optimization of Wind Farms", Renewable Energy, Vol. 36, No. 7, pp. 1973-1982, (2011).

[12] Rahbari, O., Vafaeipour, M., Fazelpour, F., Feidt, M., and Rosen, M.A., "Towards Realistic Designs of Wind Farm Layouts: Application of A Novel Placement Selector Approach", Energy Conversion and Management, Vol. 81, pp. 242-254, (2014).

[13] Feng, J., and Shen, W.Z., "Wind Farm Power Production in the Changing Wind: Robustness Quantification and Layout Optimization", Energy Conversion and Management, Vol. 148, pp. 905-914, (2017).

[14] Wan, C., Wang, J., Yang, G., and Zhang, X., "Optimal Micro-siting of Wind Farms by Particle Swarm Optimization", In International Conference in Swarm Intelligence, pp. 198-205, Springer, Berlin, Heidelberg, (2010).

[15] Chen, Y., Li, H., Jin, K., and Song, Q., "Wind Farm Layout Optimization using Genetic Algorithm with Different Hub Height Wind Turbines", Energy Conversion and Management, Vol. 70, pp. 56-65, (2013).

[16] Chen, Y., Li, H., He, B., Wang, P., and Jin, K., "Multi-objective Genetic Algorithm Based Innovative Wind Farm Layout Optimization Method", Energy Conversion and Management, Vol. 105, pp. 1318-1327, (2015).

[17] Kusiak, A., and Song, Z., "Design of Wind Farm Layout for Maximum Wind Energy Capture", Renewable Energy, Vol. 35, No. 3, pp. 685-694, (2010).

[18] Chen, L., and MacDonald, E., "A System-level Cost-of-energy Wind Farm Layout Optimization with Landowner Modeling", Energy Conversion and Management, Vol. 77, pp. 484-494, (2014).

[19] Song, M., Chen, K., and Wang, J., "A Two-Level Approach for Three-dimensional Micro-siting Optimization of Large-scale Wind Farms", Energy, Vol. 190, 116340, (2020).

[20] Wu, Y., Zhang, Sh., Wang, R., Wang, Y., and Feng, X., "A Design Methodology for Wind Farm Layout Considering Cable Routing and Economic Benefit Based on Genetic Algorithm and Geosteiner", Renewable Energy, Vol. 146, pp. 687-698, (2020).

[21] Giovanni, G., "Comparative Analysis and Improvement of Grid-based Wind Farm Layout Optimization", Energy Conversion and Management, Vol. 208, 112593, (2020).

[22] Yang, K., and Cho, K., "Simulated Annealing Algorithm for Wind Farm Layout Optimization: A Benchmark Study", Energies, Vol. 12, No. 23, 4403, (2019).

[23] ANSYS Fluent, Theory Guide. Ansys Inc (2015).

[24] Chaviaropoulos, P.K., and Hansen, M.O.L., "Investigating Three-dimensional and Rotational Effects on Wind Turbine Blades by Means of a Quasi-3D Navier-Stokes Solver", ASME Journal of Fluids and Engineering, Vol. 122, No. 2, pp. 330-336, (2000).

[25] Pape, A.L., and Lecanu, J., "3D Navier–Stokes Computations of a Stall-regulated Wind Turbine", Wind Energy, Vol. 7, No. 4, pp. 309-324, (2004).

[26] Sørensen, N.N., Michelsen, J.A., and Schreck, S., "Navier–Stokes Predictions of the NREL Phase VI Rotor in the NASA Ames 80 Ft× 120 Ft Wind Tunnel", Wind Energy, Vol. 5, No. 2- 3, pp. 151-169, (2002).

[27] Wilcox, D.C., "*Turbulence Modeling for CFD*", La Canada, DCW Industries, California (1998).

[28] Ashouri, T. A., "Computational Model for Wind Turbine Composite Blade Design and Optimization: A Finite Element Approach", M.Sc. Thesis, Sharif University of Technology, Tehran, Iran, (2005).

[29] Vermeer, L.J., Sørensen, J.N., and Crespo, A., "Wind Turbine Wake Aerodynamics", Progress in Aerospace Science, Vol. 39, No. 6-7, pp. 467-510, (2003).

[30] Whale, J., Anderson, C.G., Bareiss, R., and Wagner, S., "An Experimental and Numerical Study of the Vortex Structure in the Wake of a Wind Turbine", Wind Engineering and Industrial Aerodynamics, Vol. 84, No. 1, pp. 1-21, (2000).

[31] Lignarolo, L.E.M., Ragni, D., Krishnaswami, C., Chen, Q., Ferreira, C.S., and Van Bussel, G.J.W., "Experimental Analysis of the Wake of a Horizontal-axis Wind-turbine Model", Renewable Energy, Vol. 70, pp. 31-46, (2014).

[32] Sedaghatizadeh, N., Arjomandi, M., Kelso, R., Cazzolato, B., and Ghayesh, M.H., "Modelling of Wind Turbine Wake using Large Eddy Simulation", Renewable Energy, Vol. 115, pp. 1166-1176, (2018).

[33] Mo, J.O., Choudhry, A., Arjomandi, M., and Lee, Y.H., "Large Eddy Simulation of the Wind Turbine Wake Characteristics in the Numerical Wind Tunnel Model", Wind Engineering and Industrial Aerodynamics, Vol. 112, pp. 11-24, (2013).

[34] Sorensen, J.N., and Shen, W.Z., "Numerical Modeling of Wind Turbine Wakes", ASME Journal of Fluids Engineering, Vol. 124, No. 2, pp. 393-399, (2002).

[35] Haupt, R.L., and Haupt, S.E., "*Practical Genetic Algorithms*", 2nd Edition, John Wiley and Sons, New York, (2004).

Nomenclature

C_p	power coefficient
$\mathbf{Cost}_{total}$	wind farm cost
f	wind fraction of occurrence
N_t	number of turbines
P	output power
P_{total}	total output power of the wind farm
$\bar{p}$	mean pressure
R	blade radius
S	swept area of the blades
u^*	friction velocity
$\bar{u}_i$	mean velocity tensor
u_i'	fluctuating component of velocity
V_{hub}	wind speed at the hub height
y	wall distance
y^+	dimensionless wall distance
z_0	surface roughness
z	height of turbine tower
α	slope of wake region
μ	dynamic viscosity
ν	kinematic viscosity
ρ	air density
$\bar{\tau}_{ij}$	mean viscous stress tensor components